

Formation of the Ni₃Nb δ-Phase in Stress-Relieved Inconel 625 Produced via Laser Powder-Bed Fusion Additive Manufacturing



ERIC A. LASS, MARK R. STOUDT, MAUREEN E. WILLIAMS, MICHAEL B. KATZ,
LYLE E. LEVINE, THIEN Q. PHAN, THOMAS H. GNAEUPEL-HEROLD,
and DANIEL S. NG

The microstructural evolution of laser powder-bed additively manufactured Inconel 625 during a post-build stress-relief anneal of 1 hour at 1143 K (870 °C) is investigated. It is found that this industry-recommended heat treatment promotes the formation of a significant fraction of the orthorhombic D0_a Ni₃Nb δ-phase. This phase is known to have a deleterious influence on fracture toughness, ductility, and other mechanical properties in conventional, wrought Inconel 625; and is generally considered detrimental to materials' performance in service. The δ-phase platelets are found to precipitate within the inter-dendritic regions of the as-built solidification microstructure. These regions are enriched in solute elements, particularly Nb and Mo, due to the micro-segregation that occurs during solidification. The precipitation of δ-phase at 1073 K (800 °C) is found to require up to 4 hours. This indicates a potential alternative stress-relief processing window that mitigates δ-phase formation in this alloy. Ultimately, a homogenization heat treatment is recommended for additively manufactured Inconel 625 because the increased susceptibility to δ-phase precipitation increases the possibility for significant degradation of materials' properties in service.

DOI: 10.1007/s11661-017-4304-6

© The Minerals, Metals & Materials Society and ASM International (outside the USA) 2017

I. INTRODUCTION

ADDITIVE manufacturing (AM), as a route for commercial production of materials and components, is a potentially transformative technology because it provides a method for producing complex, three-dimensional parts with intricate geometries and internal structures that are difficult, costly, or impossible to produce *via* traditional subtractive manufacturing processes.^[1-4] Titanium alloy Ti-6Al-4V, stainless steels, and nickel-based superalloys are among the most popular alloys used for metal-based AM. These materials have been chosen primarily for the range of desirable properties (such as weldability, availability of

feedstock, *e.g.*, powder) and the widespread use within the aerospace and medical industries, which is where AM is expected to have the most immediate impact. Unfortunately, these materials are all wrought alloys that were developed within a specific framework of thermal and/or mechanical processing conditions. The conditions generated during the AM process are vastly different from those in conventional casting, forging, or welding.

Conventional casting alloys are melted and cast in a mold that has similar dimensions to the desired final product, and the cooling rate during solidification is on the order of 1 to 1000 K/s. Little secondary processing is required for most cast materials, but some can be annealed to homogenize the material and/or precipitate certain strengthening phases. Even after homogenization, remnants of the solidification microstructure (*e.g.*, crystallographic texturing or elongated, columnar grains) are sometimes observed in the microstructure of cast alloys.

Traditional wrought materials are commonly cast into a billet, which is then thermo-mechanically processed by forging, rolling, or similar process. This high temperature deformation process breaks up the dendritic solidification microstructure, homogenizes any compositional inhomogeneities arising from solidification, and facilitates

ERIC A. LASS, MARK R. STOUDT, MAUREENE WILLIAMS, MICHAEL B. KATZ, LYLE E. LEVINE, and DANIEL S. NG are with the Materials Science and Engineering Division, Material Measurement Laboratory, National Institute of Standards and Technology, Gaithersburg, MD, 20899. Contact e-mail:eric.lass@nist.gov THIEN Q. PHAN is with the Intelligent Systems Division, Engineering Laboratory, National Institute of Standards and Technology. THOMAS H. GNAEUPEL-HEROLD is with the NIST Center for Neutron Research, National Institute of Standards and Technology.

Manuscript submitted July 6, 2017.

recrystallization. For this reason, the final microstructure of a wrought alloy is typically more uniform, *i.e.*, compositionally homogeneous with an equiaxed grain structure, compared to cast alloys.

In contrast, AM processing generates cooling rates on the order of 10^3 K/s to 10^6 K/s during solidification, which are substantially higher than those in traditional cast and wrought processes. Qualitatively, the microstructures of as-built AM processed materials are similar to conventionally cast materials. Because of the slower cooling, the primary dendrite spacing in conventional cast materials is typically on the order of tens to hundreds of micrometers, whereas the higher solidification rates of AM processing produce a finer dendritic structure with primary dendrite spacing on the order of hundreds of nanometers to single micrometers.

Since the suggested thermo-mechanical processing of AM materials is typically limited to relatively low temperature stress-relief annealing, a highly micro-segregated solidification microstructure remains in the stress-relieved parts. This is quite different from the microstructures observed in wrought materials with the same nominal composition. Thus, materials produced *via* AM often exhibit highly inconsistent properties that differ dramatically from those of their wrought counterparts. For example, in wrought form 17-4 PH is a fully martensitic precipitation hardenable stainless steel with a 0.2 pct offset yield strength of 750 to 1200 MPa, an ultimate tensile strength of 1000 to 1300 MPa, and an elongation to failure of 8 to 10 pct, depending on heat treatment condition.^[5] However, AM 17-4 PH can contain a volume fraction of retained austenite in excess of 60 pct^[6] and exhibits a yield strength of less than 500 MPa and an elongation to failure of up to 20 pct.^[7] In some cases, one or more of the properties may be similar in both AM and conventionally-produced materials while others are appreciably different. For example, the ultimate tensile strength and yield stress of AM Inconel 625 (IN625) have been reported to be comparable to wrought IN625, but the elongation to failure, particularly at elevated temperatures, of the AM material is less than half that of the wrought.^[8] These observations can be readily explained in terms of the materials engineering tenet of “processing-structure-property relationships”. To date, much of the AM literature has focused on the relationships between AM processing and materials properties, where the “structure” linkage, and specifically the microstructure, is minimized or ignored altogether. Clearly, a material developed for one set of processing parameters cannot be expected to exhibit identical properties when fabricated by an alternative production method.

Inconel 625 (IN625) is a widely-used Ni-based superalloy. In wrought form, the mechanical strength is derived primarily from solid solution strengthening *via* alloying with Cr, Mo, and Nb. Additional strengthening has been reported for certain compositions and conditions *via* precipitation of the metastable body-centered tetragonal D0₂₂ Ni₃Nb γ'' -phase.^[9–11] Formation of the orthorhombic D0_a Ni₃Nb δ -phase is also possible in any alloy where precipitation strengthening by γ'' is possible, including IN625^[9–11] and Inconel 718.^[11,12] Both γ'' and

δ are known to form in conventional solid solution strengthened IN625 when it is exposed to elevated temperatures for extended periods of time (*i.e.*, hundreds to thousands of hours). Precipitation of γ'' occurs at lower temperatures, 823 K to 1023 K (550 °C to 750 °C), while δ forms at higher temperatures, 1023 K to 1253 K (750 °C to 980 °C).^[9–11] However, δ is the equilibrium phase, and given enough time, any metastable γ'' that forms will ultimately transform to δ .^[9] Although some evidence suggests that controlled formation of δ can enhance tensile strength^[11] and microhardness,^[13] it is generally considered an undesirable precipitate phase because its formation is known to decrease both the fracture toughness and the ductility.^[9,11,13,14]

IN625 is also known to exhibit excellent weldability,^[9–11] which is one of the properties that make it attractive for AM. However, the segregation of solute elements during solidification in the welding process increases the likelihood for the precipitation of secondary phases, including both γ'' and δ , Laves phases, and several carbide phases.^[15,16] Similar effects have also been observed in rapidly solidified IN625.^[17]

The as-fabricated microstructure of AM-produced IN625 is strongly influenced by the type of AM process used. Electron-beam (powder-bed) melting (EBM) generates a columnar grain structure with a strong (100) texture along the solidification (*i.e.*, build) direction.^[18] The primary cell/dendrite spacing of EBM produced IN625 is on the order of a few micrometers. Within the as-built microstructure, plate-like second-phase precipitates are observed along the vertically aligned inter-dendritic regions. During the EBM process, the build plate is typically heated to as high as 1073 K (800 °C), which tends to “anneal” the material and promote the formation of these precipitate phases.^[19] Murr *et al.*^[18] identified these precipitates as γ'' *via* transmission electron microscopy (TEM). Further evaluation of their x-ray diffraction (XRD) patterns reveal a peak at 46° 2θ in their Figures 5(a) and (b). This peak suggests δ may also be present in their material.

Laser-based AM of IN625 has also been investigated. Dinda *et al.*^[20] studied the microstructure of laser direct metal deposition (L-DMD) of IN625, where powder is fed into a laser beam (as opposed to powder-bed). They reported a similar solidification microstructure to that found in EBM with a primary dendrite spacing on the order of 5 μm and secondary dendrite arm spacing of about 2 μm . Their analysis of material annealed for 1 hour at temperatures between 973 K and 1473 K (700 °C and 1200 °C) was limited to optical microscopy, XRD, and microhardness measurements. While they found no direct evidence of either γ'' or δ , they attributed the observed changes in the measured microhardness and FCC lattice parameter between the as-built and annealed materials to the formation and dissolution of these two phases.

Recently, Zhang *et al.*^[21] investigated the microstructure of IN625 produced using laser powder-bed fusion (L-PBF). They observed a finer cellular/dendritic solidification microstructure than that observed in either EBM or L-DMD, with a primary dendrite spacing of

about 1 μm . This suggests that the cooling process in L-PBF is more rapid than in EBM or L-DMD. They also demonstrated significant segregation of Nb and Mo to the inter-dendritic regions, while the dendrite cores were enriched in Ni and Cr. Recent Calphad and phase-field modeling has also suggested significant micro-segregation in IN625 produced using L-PBF AM.^[22] Zhang *et al.* did not investigate secondary phases, but investigated the homogenization behavior of the highly micro-segregated solidification microstructure. They reported that a homogenization heat treatment of 30 to 60 minutes at 1423 K (1150 °C) was sufficient to relieve the solidification micro-segregation. Kreitberg *et al.*^[8,23] also investigated the effect of post-build thermal processing on the microstructure and mechanical properties of L-PBF produced IN625. In their first publication, they mention “ Ni_3Nb ” in their discussion but do not specify whether it is γ' or δ and provide no evidence for the existence of either phase. In a very recent publication, they identify these precipitates as delta.^[23] They reported elongated grains and (100) texturing along the build direction, which produced anisotropy in the mechanical behavior. This anisotropy was increasingly mitigated by heat treatment at increasing temperatures, and nearly eliminated after hot isostatic pressing (1393 K to 1513 K (1120 °C to 1240 °C), 100 to 165 MPa, 3 to 4 hours).

The present work investigates the effects of post-build stress-relief heat treatment on the microstructure of L-PBF produced IN625. Because this build process can generate residual stresses that approach the yield strength of IN625, a stress-relief annealing step is typically required prior to removal of the components from the build plate. EOS*, a manufacturer of L-PBF

*Mention of commercial products does not imply endorsement by the National Institute of Standards and Technology, nor does it imply that such products or services are necessarily the best available for the purpose.

equipment, suggests a stress-relief heat treatment of 1 hour at 1143 K (870 °C) for AM IN625. The microstructures of as-built and stress-relieved material are characterized, revealing the formation deleterious phases during the industry-recommended stress-relief protocol. Additional annealing conditions are also investigated as potential alternatives to current practice as a method of mitigating the formation of deleterious secondary phases during stress-relief annealing.

II. EXPERIMENTAL PROCEDURE

Fifteen millimeter cubes were additively-produced from virgin IN625 powder using an EOS M270 L-PBF system and a standard EOS parameter set for IN625. The composition of the powder feedstock is given in Table I. The parameter set included a laser power of 195 W, a scan speed of 800 mm s⁻¹, a nominal powder layer thickness of 20 μm , and a hatch spacing of 100 μm . An “all core” build pattern was used, *i.e.*, the

Table I. Composition of the IN625 Powder Feedstock Used to Produce the AM Parts Investigated in the Present Study

| Element | Mass Fraction ($\times 100$) |
|---------|--------------------------------|
| Ni | balance |
| Cr | 20.70 |
| Mo | 8.83 |
| Nb | 3.75 |
| Fe | 0.72 |
| Ti | 0.35 |
| Al | 0.28 |
| Co | 0.18 |
| Mn | 0.03 |
| C | 0.01 |
| Si | 0.13 |
| P | <0.01 |
| S | 0.002 |

No uncertainty was provided by the manufacturer.

laser scan pattern was identical at the external surfaces and in the interior of the samples. The samples were cut from the build plate *via* electro-discharge machining in the as-built condition, *i.e.*, without undergoing any stress-relief heat treatment. Samples of the as-built AM IN625 were then sealed in evacuated and Ar-backfilled quartz ampules for heat treatment.

The encapsulated samples were annealed at 1143 K (870 °C) for 1 hour, following the manufacturer-recommended stress-relief protocol. Samples were also annealed at 1073 K (800 °C) for 1 and 4 hours. Portions of the as-built and heat-treated material were mounted and polished using standard metallographic techniques for scanning electron microscopy (SEM) analysis.^[24] A final polishing step using a vibrational polishing system with 0.2 μm colloidal silica was employed to provide a strain-free surface for SEM and energy dispersive X-ray spectroscopy (EDS). The samples were also etched *via* immersion in aqua regia for 10 to 60 seconds to reveal the microstructure. Thin foils of the heat-treated material were prepared for TEM analysis by mechanical thinning to about 150 μm followed by twin-jet electropolishing in a solution of 6 pct perchloric acid in methanol at a temperature of 253 K (−20 °C). Laboratory-based XRD analysis was performed using Cu $K\alpha$ radiation on the as-built and annealed samples after the surfaces were polished to a 1 μm diamond finish. A scan range of 20° to 100° 2θ was used to identify all phases existing in the samples. The range of 30° to 60° 2θ was further chosen for more detailed investigation focusing on the δ -phase peaks of interest.

The procedure of neutron stress measurements followed closely the one described in Reference 25 where samples with similar geometry and properties were investigated. Here, neutron diffraction stress measurements were done using the (311) reflection at a constant wavelength of $\lambda = 1.5877 \text{ \AA}$. The nominal spatial resolution was 1 mm × 1 mm × 1 mm (gage volume), with measurement locations arranged in the pattern shown in the sketch (Figure 1). The d -spacings were obtained in the three principal directions (x,y,z) through appropriately orienting the sample. The conversion to lattice strains for stress calculation also required an

estimate for the unstressed d -spacing d_0 , which was obtained from the two measurements near the top and bottom surface (support layer). At these two locations, the condition $\sigma_{zz} = 0$ is applicable, and d_0 can be calculated such that $\sigma_{zz} = 0$ (plane stress condition).

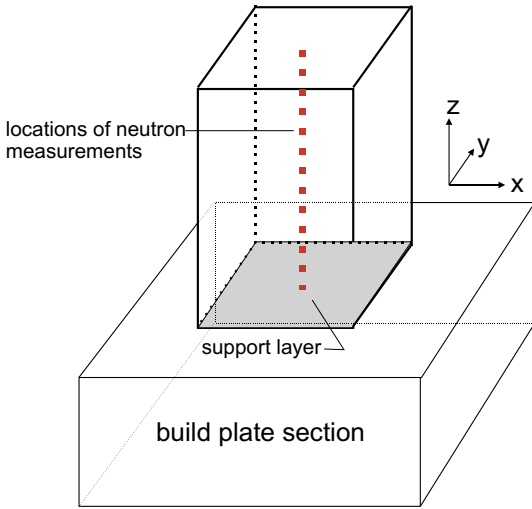


Fig. 1—Schematic of the specimen geometry used for the neutron diffraction experiments.

III. RESULTS AND DISCUSSION

A. As-Built and Stress-Relieved AM IN625

Figures 2(a) and (b) present SEM images of the as-built IN625 microstructure. The microstructure is dendritic with a primary dendrite spacing on the order of $1\ \mu\text{m}$. The secondary dendrite arm spacing is approximately $300\ \text{nm}$; however, the secondary dendrites are not easily differentiated because the high solidification rate is near the transition point between dendritic and cellular solidification. Figure 3 presents EDS composition maps showing the Ni, Cr, Nb, Mo, and C concentrations for an area of the as-built microstructure. These maps reveal that the dendrite cores (the darker, etched away regions in Figure 2) are enriched in Ni and Cr; while the inter-dendritic regions (the brighter, un-etched regions in Figure 2) are enriched in the solute elements Nb and Mo. The XRD results presented in Figure 2(c) exhibit no identifiable peaks other than those of the FCC phase, confirming that the microstructure is almost entirely a single-phase, though inhomogeneous, FCC solid solution.

Figure 4 shows the microstructure after a recommended stress-relief heat treatment. The microstructure has been dramatically altered compared to that of the as-built material. Many bright, plate-like precipitates covering the entire microstructure are observed. These precipitates are primarily aligned in a columnar fashion,

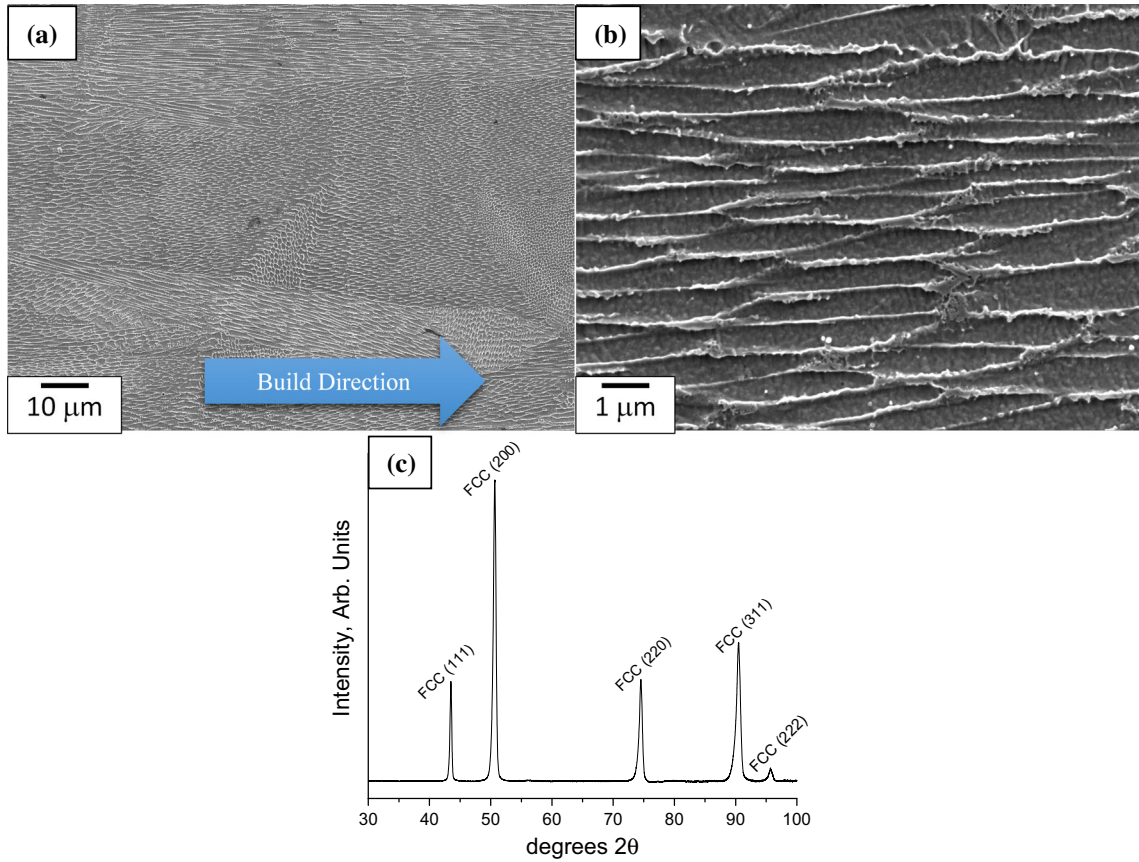


Fig. 2—(a) and (b) Microstructure of the as-built AM IN625. (c) XRD pattern from the same sample. The only phase identified in the XRD pattern is FCC.

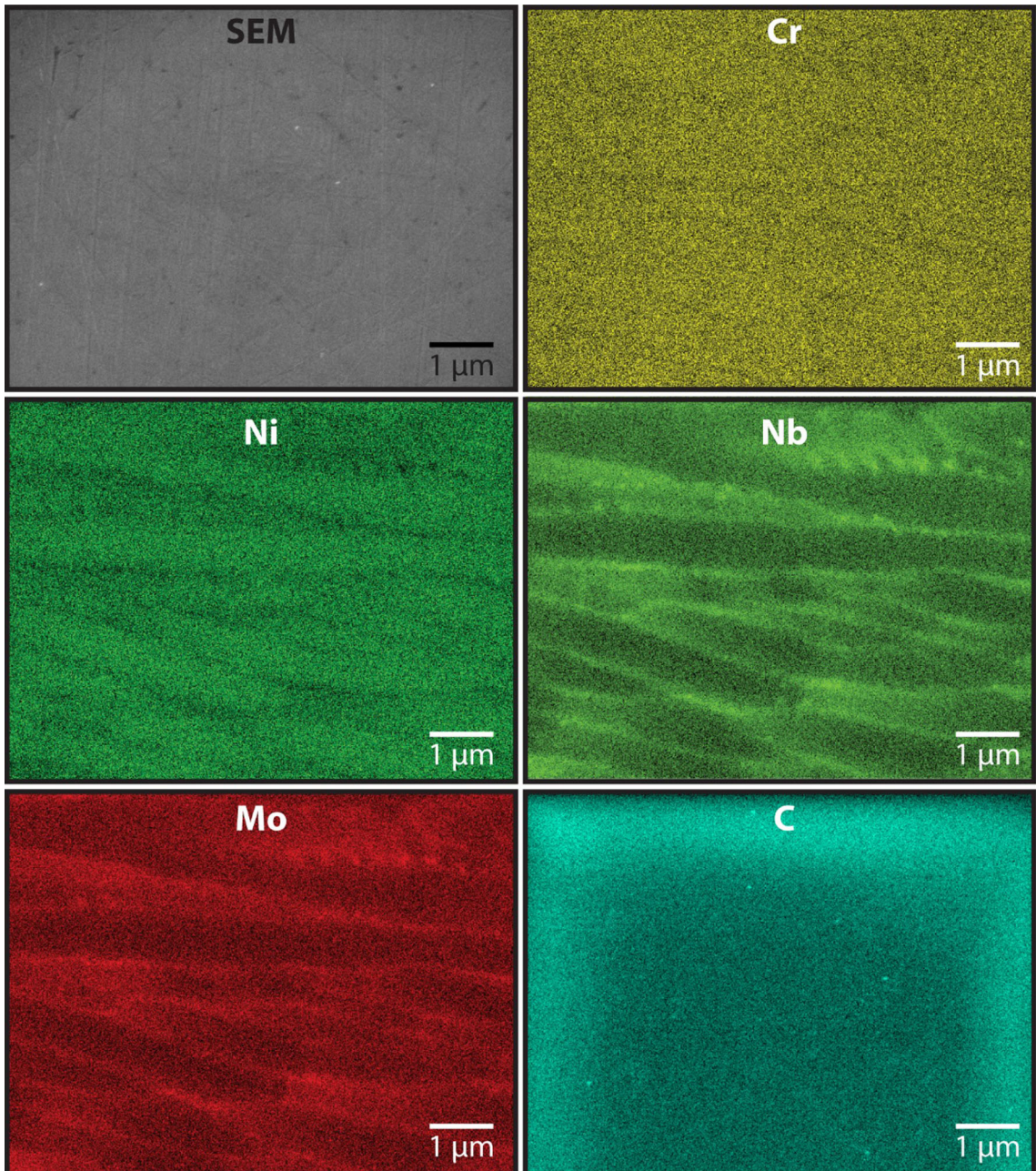


Fig. 3—EDS compositional map of Cr, Ni, Nb, Mo, and C of the as-built microstructure of AM IN625. The bright outline in the C map is an artifact arising from the C-based sample mounting material.

along the solute-rich inter-dendritic regions. The XRD pattern of the AM IN625 material annealed at 1143 K (870 °C) for 1 hour, Figure 4(c), shows the presence of several peaks in addition to the FCC matrix peaks. Specifically, an additional peak is observed at $40.8^\circ 2\theta$ as well as a two-peak doublet near $46^\circ 2\theta$. This peak doublet is also present in the XRD patterns of Murr *et al.*^[18] These peaks are associated with the orthorhombic Ni_3Nb δ -phase. The EDS maps in Figure 5 illustrate that the precipitates are depleted in Cr and enriched in Nb and Mo. Digital image analysis (thresholding) of the stress-relieved microstructure in 4b, yields an areal fraction of the δ -phase of about (9 ± 3) pct (the

uncertainty is estimated from previous experience of areal fraction determination *via* digital image analysis, and represents approximately two standard deviations of several independent measurements). It should be noted that because of the plate-like morphology of the δ -phase precipitates and thicknesses on the order of a few tens of nanometers, the δ -phase fraction determined *via* image analysis is likely an upper bound on the true volume fraction.

The precipitation of δ -phase is known to occur in IN625 after exposure to elevated temperatures for periods of time on the order of hundreds of hours,^[9,13,14] though some more recent results suggest its precipitation

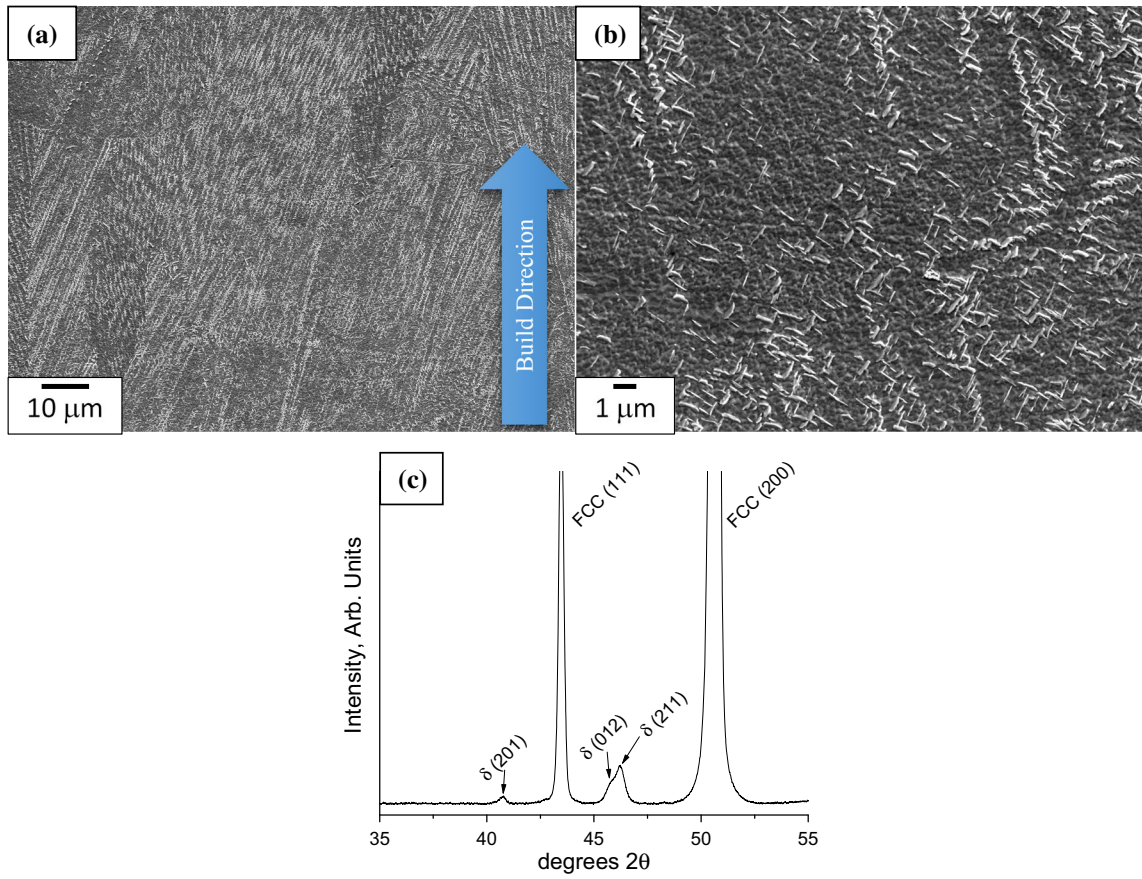


Fig. 4—(a) and (b) Microstructure of AM IN625 after stress-relief heat treatment of 1 h at 1143 K (870 °C). (c) XRD pattern from the same sample exhibiting multiple peaks corresponding to δ -Ni₃Nb.

may be as early as about 10 hours.^[10,26] Never-the-less, the formation of δ -phase after 1 hour at 1143 K (870 °C) is more rapid than expected for wrought IN625. Applied stress has also been shown to increase the precipitation kinetics of δ -phase in wrought IN625.^[10,26] Although residual stresses are present in the as-built microstructure, the observed preferential precipitation along the Nb-rich inter-dendritic regions of the solidification microstructure strongly suggests the more rapid δ -phase precipitation is caused by these compositional fluctuations producing regions of locally enhanced precipitation conditions. This is supported by similar observations of δ -phase formation along Ni-enriched interdritic regions of the solidification microstructure in IN625 welds^[9,15,16] and rapidly solidified IN625 ribbon^[17] after similarly short periods of time.

Figure 6 presents TEM micrographs and a selected area electron diffraction (SAED) pattern of one precipitate in the stress-relieved material. This confirms that the plate-like precipitates observed in this condition are δ -phase. The orientation relationship between the FCC matrix and δ precipitates is the same as that found in wrought IN625 after prolonged exposure at elevated temperature,^[11] expressed as

$$\{111\}_{\gamma} \parallel (100)_{\delta}; \quad \langle 1\bar{1}0 \rangle_{\gamma} \parallel [100]_{\delta}.$$

It should also be noted that evidence of metastable γ'' was also found in the TEM investigation of the AM IN625 material after stress relieving at 1143 K (870 °C) for 1 hour. However, no evidence for this phase is observable in the XRD pattern of Figure 4(c). The presence of this phase in the stress-relieved sample is somewhat surprising considering that γ'' is typically observed at temperatures below approximately 1023 K (750 °C) in wrought IN625. A rationale for the formation of γ'' in AM IN625 at 1143 K (870 °C) is outside the scope of the present discussion and will be the subject of a future report. The results of the present analysis suggest that the highly micro-segregated solidification microstructure creates a local environment within the inter-dendritic regions where growth of γ'' is competitive with that of δ at temperatures where γ'' is not observed in wrought IN625.

B. Stress-Relief Alternatives

As mentioned above, δ is known to form in wrought IN625 after extended periods of time at elevated

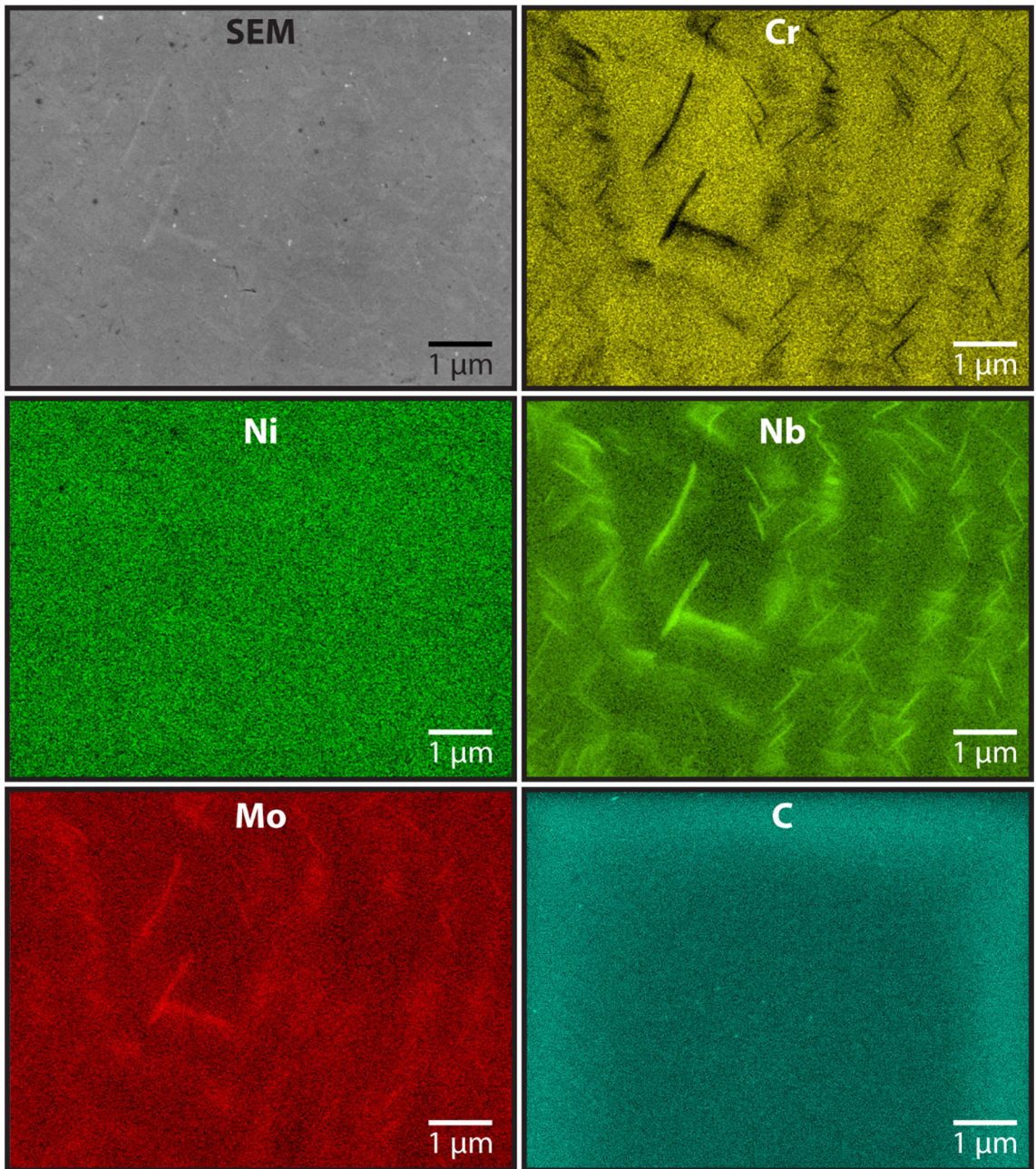


Fig. 5—EDS mapping of Cr, Ni, Nb, Mo, and C of the microstructure of AM IN625 after a stress-relief annealing heat treatment at 1143 K (870 °C) for 1 h. The bright outline in the C map is an artifact arising from the C-based sample mounting material.

temperatures, and its presence has a detrimental effect on mechanical properties such as ductility and fracture toughness. Here we show that by simply following the industry-recommended stress-relief heat treatment, a large volume fraction of δ forms because of the significant micro-segregation found in the solidification microstructure of the as-built AM IN625. However, in an industrial setting, a stress-relief heat treatment is likely necessary to remove the AM parts from the build plate.

The SEM micrograph (Figure 7(a)) and XRD pattern (Figure 7(c)) demonstrated that the microstructure of AM IN625 annealed at 1073 K (800 °C) for 1 hour has

no significant δ -phase formation. The EDS composition maps for the sample annealed at 1073 K (800 °C) for 1 hour, shown in Figure 8, are similar to those for the as-built material, Figure 2, except the inter-dendritic regions are slightly enriched in C in addition to Nb and Mo. The presence of C with the Nb and Mo suggest the formation of carbide phases, such as MC or M_6C , instead of δ . It is possible that some of the brightest Nb/Mo spots in the micrograph could be small δ -phase precipitates. Closer inspection of the Ni map reveals that these spots are Ni-poor, which is consistent with the formation of Nb- and Mo-rich carbides phases rather than δ . Regardless, the volume fraction of δ in the

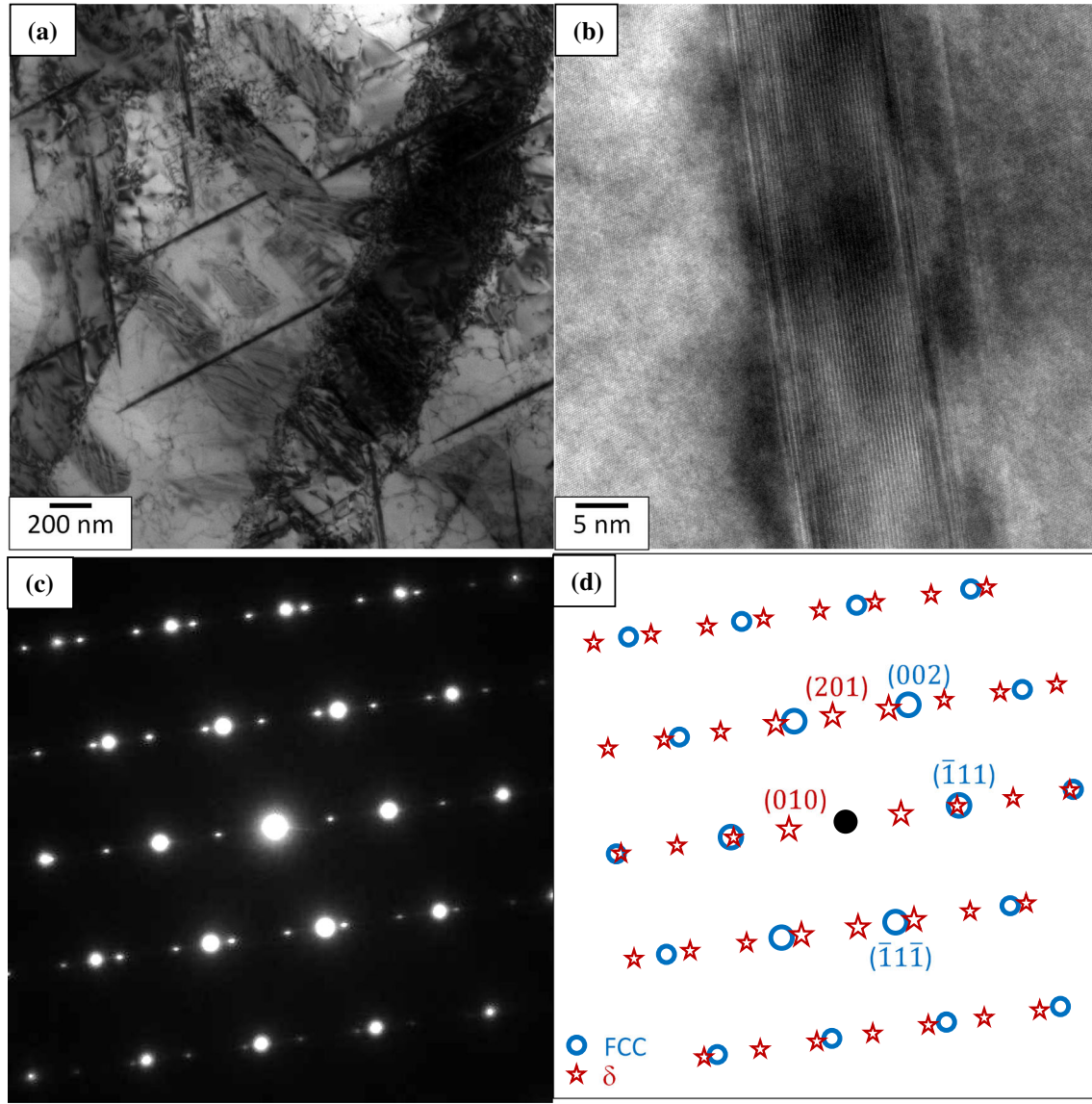


Fig. 6—(a) Bright field TEM micrograph of δ -phase in an FCC matrix in the AM IN625 annealed at 1143 K (870 °C) for 1 h. (b) High resolution TEM micrograph of a δ plate edge on. (c) selected area diffraction pattern of one δ precipitate (within an FCC matrix), and (d) the key to the SAED pattern in (c) identifying the spots associated with the FCC matrix and δ precipitates.

sample annealed at 1073 K (800 °C) for 1 hour is <1 pct. Figure 7(b) (and the XRD patterns in c) reveal that some δ forms after 4 hours at 1073 K (800 °C), about (6 ± 3) pct. However, the fraction is lower than that formed after 1 hour at 1143 K (870 °C).

Neutron diffraction results, presented in Figure 9, suggest that annealing as-built AM IN625 for 1 hour at 1073 K (800 °C) reduces the residual macro-stresses to approximately 25 pct (≈ 200 MPa, Figure 9(c)) of those in the as-built condition (≈ 800 MPa, Figure 9(a)). By comparison, the manufacturer-recommended stress-relief heat treatment [1 hour at 1143 K (870 °C)], reduces the residual macro-stresses to about 13 pct (≈ 100 MPa, Figure 9(b)) of the as-built material. These neutron diffraction residual stress measurements and the microstructural evolution investigation together suggest that a temperature of 1073 K (800 °C) may offer a

potential alternative stress-relief heat treatment option. Note that it is unclear whether the residual stress reduction produced after annealing for 1 hour at 1073 K (800 °C) is sufficient to allow removal of the parts from the build plate. However, the results do suggest that extending the annealing time at 1073 K (800 °C) could further reduce the residual stresses without forming significant amounts of δ . Indeed, preliminary results suggest that the volume fraction of δ present after annealing for 2 hours at 1073 K (800 °C) is only about (1.0 ± 0.5) pct.

C. Further Thermal Processing and δ -Phase Removal

Once it has formed, removal of the δ -phase may require extended periods of time at temperatures above 1373 K (1100 °C). Floreen *et al.*^[9] reported that

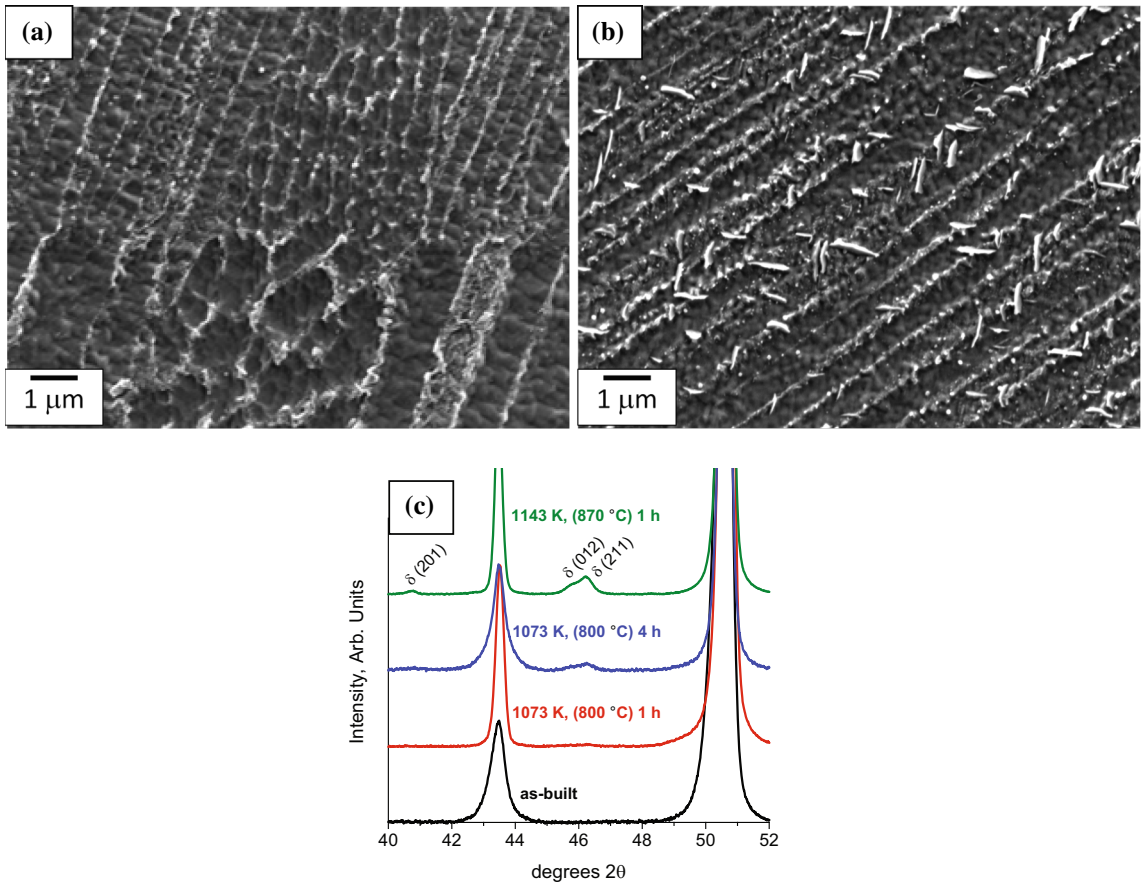


Fig. 7—Microstructure of AM IN625 after annealing at 1073 K (800 °C) for (a) 1 h and (b) 4 h; and (c) XRD patterns of the samples shown in (a) and (b), compared to the as-built and 1143 K (870 °C), 1 h annealed material.

dissolution of δ in wrought IN625 requires up to 24 hours at 1373 K (1100 °C). In contrast, Shankar *et al.*^[13] suggest that 30 minutes at 1423 K (1150 °C) is sufficient to eliminate δ -phase. Furthermore, the highly segregated microstructure and large composition gradients in the as-built condition could significantly affect δ -phase dissolution. Additional studies are in progress to determine the relationship between heat treatment and the dissolution of δ in an AM IN625 microstructure. Zhang *et al.*^[21] recently demonstrated that annealing for 30 to 60 minutes at 1423 K (1150 °C) effectively homogenizes the solidification microstructure of AM IN625. Whether this protocol is sufficient when δ is present is not yet clear. It should also be noted that the stress-relief heat treatments in the present work are idealized laboratory experiments, performed on small specimens. In an industrial setting, heating and cooling rates, soak times at temperature, and thicker specimen geometries will result in a variation in stress-relief annealing conditions, which must be taken into consideration. Regardless, because of the enhanced propensity for δ -phase formation in the as-built AM IN625 microstructure, a homogenization heat treatment is strongly recommended prior to the use of AM IN625 in any real-world application. This is particularly important for an application at elevated temperatures,

to ensure microstructural stability and consistent properties while in service.

IV. CONCLUSIONS

An industry-recommended stress-relief heat treatment protocol of 1 hour at 1143 K (870 °C) has been demonstrated to promote the formation of a significant volume fraction, 5 to 10 pct, of the orthorhombic Ni_3Nb δ -phase in laser powder-bed additively manufactured Inconel 625. This deleterious phase is known to form after hundreds to thousands of hours at elevated service temperatures in conventional Ni-based superalloys. The enhanced susceptibility toward δ -phase precipitation in additively-produced Inconel 625 is attributed to the highly heterogeneous solidification microstructure, where the local concentrations of Nb and Mo within inter-dendritic regions can be significantly greater than that of the bulk alloy. The formation of δ is slower at 1173 K (800 °C), requiring up to 4 hours, providing a potential alternative heat treatment window where residual stresses may be sufficiently relieved while mitigating the formation of δ . Finally, because of the propensity of as-built

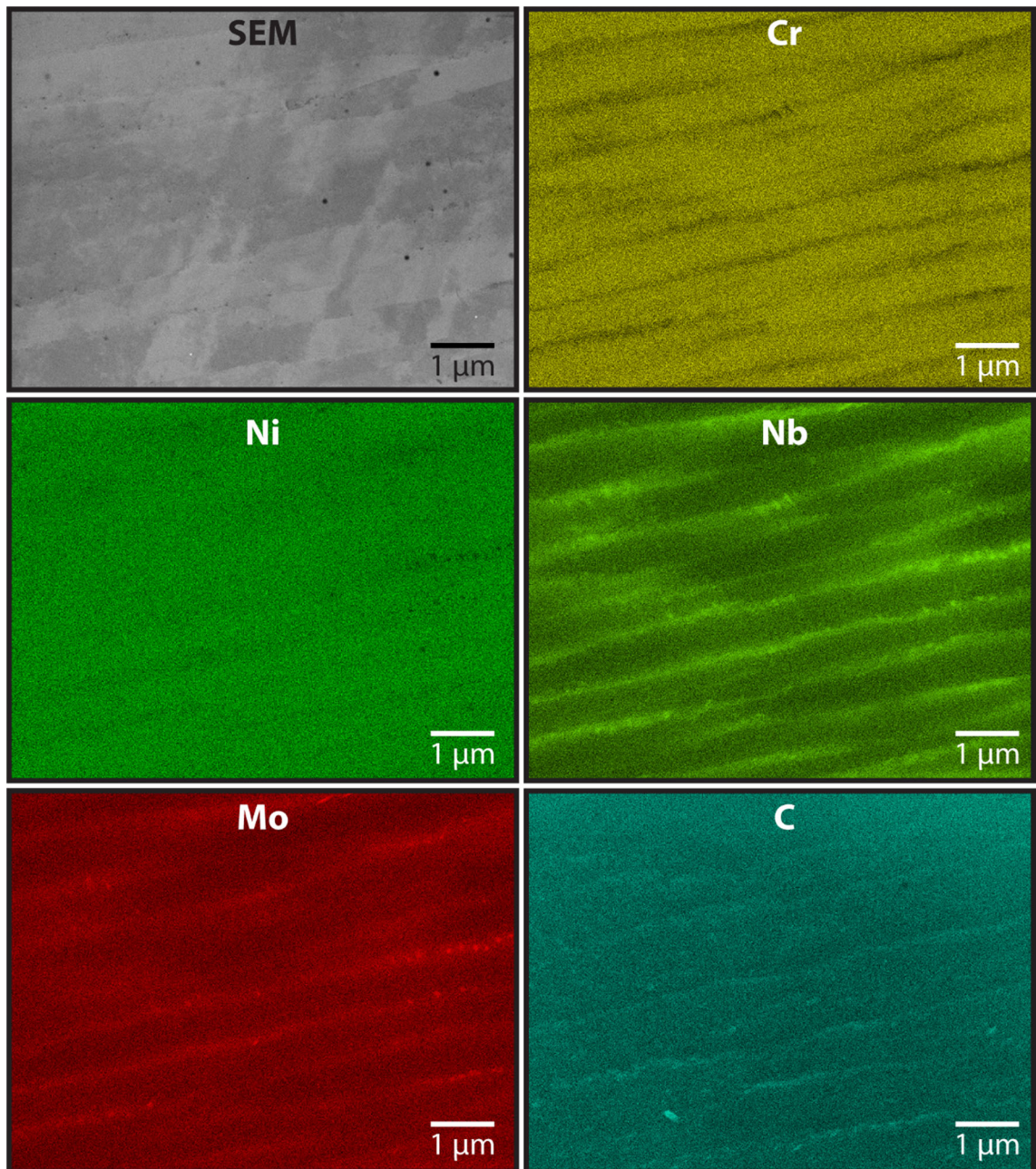


Fig. 8—EDS mapping of Cr, Ni, Nb, Mo, and C of the microstructure of AM IN625 after a heat treatment at 1173 K (800 °C) for 1 h.

additively manufactured Inconel 625 to form δ -phase, it is recommended that regardless of whether precipitation is avoided during stress-relief, a homogenization

heat treatment should be included as a post-build thermal processing step to ensure microstructural stability of the material in service.

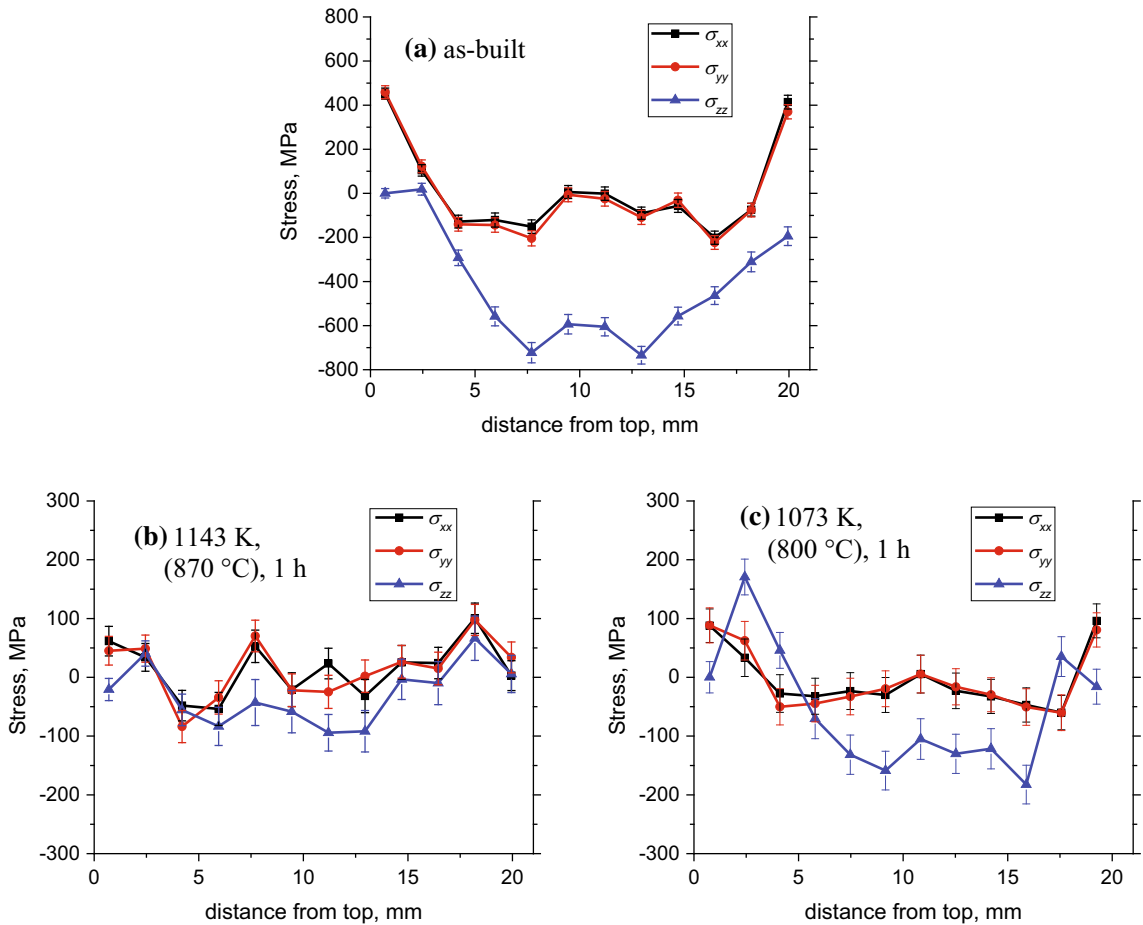


Fig. 9—Residual stresses measured via neutron diffraction in AM IN625 in (a) the as-built condition, and after stress-relief annealing at (b) 1143 K (870 °C) for 1 h, and (c) 1073 K (800 °C) for 1 h. The error bars represent the uncertainty in the lattice parameter measurements determined by fitting a Gaussian function to the neutron scattering data.

ACKNOWLEDGMENTS

The authors would like to acknowledge the Engineering Laboratory at NIST for building the IN625 samples used in this study.

REFERENCES

- G.N. Levy, R. Schindel, and J.P. Kruth: *CIRP Annals - Manuf. Tech.*, 2003, vol. 52, pp. 589–609.
- D.D. Gu, W. Meiners, K. Wissenbach, and R. Poprawe: *Int. Mater. Rev.*, 2012, vol. 57, pp. 133–64.
- L.E. Murr, E. Martinez, K.N. Amato, S.N. Gaytan, J. Hernandez, D.A. Ramirez, P.W. Shindo, F. Medina, and R.B. Wicker: *J. Mater. Res. Technol.*, 2012, vol. 1, pp. 42–54.
- R.M. Mahmood, E.T. Akinlabi, M. Shukla, and P. Pityana: *Lasers Eng.*, 2014, vol. 27, pp. 161–78.
- ATI technical data sheet, Stainless steel AL 17-4TM precipitation hardening alloy. <http://www.specialtysteelsupply.com/brochure/17-4-technical-data.pdf>. Accessed July 19, 2017.
- S. Cheruvathur, E.A. Lass, and C.E. Campbell: *JOM*, 2016, vol. 68, pp. 930–42.
- W.E. Luecke and J.A. Slotwinski: *J. Res. Natl. Inst. Stand. Technol.*, 2014, vol. 119, pp. 398–418.
- A. Kreitberg, V. Brailovski, and S. Turenne: *Mater. Sci. Eng. A*, 2017, vol. 689, pp. 1–10.
- S. Floreen, G.E. Fuchs, and W.J. Yang: in *Proceedings of Superalloys 718, 625, 706 and Various Derivatives*, E.A. Loria, ed., The Minerals, Metals & Materials Society, Pittsburgh, 1994.
- L.M. Suave, J. Cormier, P. Villechaise, A. Soula, Z. Hervier, D. Bertheau, and J. Laigo: *Metall. Mater. Trans. A*, 2014, vol. 45A, pp. 2963–82.
- M. Sundararaman, P. Mukhopadhyay, and S. Banerjee: *Metall. Trans. A*, 1968, vol. 19A, pp. 453–65.
- Y. Idell, L.E. Levine, A.J. Allen, F. Zhang, C.E. Campbell, G.B. Olson, J. Gong, D.R. Snyder, and H.Z. Deutchman: *JOM*, 2016, vol. 68, pp. 950–59.
- V. Shankar, K. Bhanu Sankara Rao, and S.L. Mannan: *J. Nuclear Mater.*, 2001, vol. 288, pp. 222–32.
- J. Mittra, S. Banerjee, R. Tewari, and G.K. Dey: *Mater. Sci. Eng. A*, 2013, vol. 574, pp. 86–93.
- X. Xing, X. Di, and B. Wang: *J. Alloys Compds.*, 2014, vol. 593, pp. 110–16.
- H.R.R. Ashtiani and R. Zarandooz: *Int. J. Manuf. Technol.*, 2016, vol. 84, pp. 607–19.
- G.K. Dey, A. Albert, D. Srivatava, M. Sundararaman, P. Mukhopadhyay: *Mater. Sci. Eng. A*, 1999, vol. 119, pp. 175–84.
- L.E. Murr, E. Martinez, S.M. Gaytan, D.A. Ramirez, B.I. Machado, P.W. Shindo, J.L. Martinez, F. Medina, J. Wooten, D. Ciscel, U. Ackelid, and R.B. Wicker: *Metall. Mater. Trans. A*, 2011, vol. 42A, pp. 3491–3508.
- Arcam technical brochure: *Just add*, Arcam AB, Mölndal, Sweden, 2017.
- G.P. Dinda, A.K. Dasgupta, and J. Mazumder: *Mater. Sci. Eng. A*, 2009, vol. 509, pp. 98–104.
- F. Zhang, L.E. Levine, A.J. Allen, C.E. Campbell, E.A. Lass, S. Cheruvathur, M.R. Stoudt, M.E. Williams, and Y. Idell: *Scripta Mater.*, 2017, vol. 131, pp. 98–102.

22. T. Keller, G. Lindwall, S. Ghosh, L. Ma, B.M. Lane, F. Zhang, U.R. Kattner, E.A. Lass, J.C. Heigel, Y. Idell, M.E. Williams, A.J. Allen, J.E. Guyer, and L.E. Levine: *Acta Mater.*, 2017, DOI:[10.1016/j.actamat.2017.05.003](https://doi.org/10.1016/j.actamat.2017.05.003).
23. A. Kreitberg, V. Brailovski, and S. Turenne: *Mater. Sci. Eng. A*, 2017, vol. 700, pp. 540–53.
24. G.F. VanderVoort: *Metallography Principles and Practice*, ASM International, Materials Park, OH, 1999.
25. T. Gnäupel-Herold, J. Slotwinski, and S. Moylan: *AIP Conf. Proc.*, 2014, vol. 1582, pp. 1205–14.
26. L.M. Suave, J. Cormier, D. Bertheau, P. Villechaise, A. Soula, Z. Hervier, and J. Laigo: *Mater. Sci. Eng. A*, 2016, vol. 650, pp. 161–70.